MOTION OF THE CELLO BRIDGE

A Zhang University of Cambridge, Department of Engineering, Cambridge, UK
J Woodhouse University of Cambridge, Department of Engineering, Cambridge, UK

1 INTRODUCTION

The bridge on most bowed string instruments is made from a special grade of maple. It is held in place only by the tension of strings and plays a critical transfer role between the vibrating strings and the radiating corpus during the sound production of the instrument. An intelligently cut and well fitted bridge can have a profound influence on the inherent tonal characteristics of bowed string instruments. Knowledge collected up to 1993 on the physics of the bridge has been summarized by Hutchins [1]. However, the cello bridge, which is very different from a violin bridge in proportions, has been less emphasized in the violin acoustics literature. This paper intends to confirm and expand previous knowledge of the motion of a cello bridge in the low- to mid-frequency range. Mechanical admittance measurements at five points around the bridge plus four points on the top plate near the bridge feet were carried on the tested cellos. The motions of these points at any given frequency were processed to show the best-fitted rigid-body motion of the bridge, which can be expressed as rotation around an instantaneous centre.

2 FUNCTION OF THE BRIDGE

Makers and researchers have been aware of the importance of the bridge for centuries. The motion of the bridge is of special interest to scientists since the energy transfer between the strings and the resonant body of the instrument is intimately affected by this motion. Minnaert [2] reported the first detailed investigation into the flexural, torsional and transverse vibration of a violin bridge using a special designed optical system. The first study on the motion of a cello bridge was done by Bladier [3] in 1960 using a piezoelectric transducer fastened to the tested bridge. In this way, he showed differences between the motions at the two cello bridge feet. In 1979, Reinicke [4] displayed the motion of a violin bridge and a cello bridge using hologram interferometry, and modelled the motions mathematically. Experiments on the motion of the violin bridge were made by Müller [5] in 1979. He measured the sound pressure with differently-designed bridges and discussed the function of the bridge. Cremer [6] summarized this work in his remarkable book of the knowledge about the violin family up to 1983. Trott [7] sketched the impedance coupling between the strings and the bridge for the first time. Marshall [8] pointed out that the violin bridge shows more motion over the bass bar area up to 700 Hz. Since the 1990's, finite element analysis has found application for studying the vibration behaviour of bowed string instruments. Studies by Rodgers and Masino [9] and Kishi and Osanai [10] both examined the bridge motion under different conditions using finite element analysis. Jansson [11, 12, 13] and his co-workers investigated the effect of bridge modification on the vibrational behaviour of the instrument. They started with the influence of wood removal from different areas of the bridge and then turned their attention to the bridge foot spacing. Modal and acoustical measurements for analyzing the motion of the violin bridge as a filter were done by Bissinger [14]. His experimental results showed the transition of the predominant motion of a violin bridge from the bass-bar side to the soundpost side, which also confirmed the findings of Marshall.

3 EXPERIMENTS

Systematic experiments have been conducted on a cello in good playing order, fitting with a Belgian design bridge but with a normal heart. Compared to the typical Belgian bridge, the bridge on the tested cello has a less compact heart. It still has an upper body and longer feet as normal Belgian ones, which contribute to produce a brighter and louder sound. The width between its outside foot-edges is 90 mm.

During the measurements, the tested cello was held by a steel support frame with a firm base and steadied firmly by soft foam pieces from two sides as shown in Figure 1. Its endpin was fixed in one hole of a centre metal strip and the neck was fastened by a cable tie to another strip above. All the acoustical measurements were undertaken in the same laboratory acoustic environment. A miniature instrumented hammer was adopted to provide a force pulse to each point of interest on the cello bridge or top plate of the tested cello. The vibration response was measured by an accelerometer mounted on the C-string corner of the cello bridge, aligned along the bowing direction of that string.

Figure 1 Cello set up for input admittance measurements.

Figure 2 shows the positions and directions for measuring the transfer admittance of the marker points on the cello bridge. The C-string corner of the cello bridge is denoted as Point 1. Points 2, 3, 4, 5 are marked by black circles on the surface of the cello bridge in its plane. Points A, B denoted by blue circles are equally spaced by the two sides of the bass-bar bridge foot on the top plate; Points C, D marked by blue circles are near the sound-post bridge foot in the same way. These nine different points were hit by the hammer in turn. Black triangles N1, N2, N3 and N4 denote the positions of the notches under the C, G, D, and A strings respectively.

Hammer impacts were only exerted in the plane of the bridge or the planes parallel to it during the measurements. Forces labelled as F1 and F3 were applied to Points 1 and 3 on the bridge along the bowing direction of the nearest strings. Impulses labelled as F2, F4 and F5, were applied to Points 2, 4, and 5 normally on the sides of the bridge, in the direction of the red arrows. Impact forces FA, FB, FC and FD were respectively imposed downward to the top plate along the directions of the blue arrows, which are normal to the top plate. Because Points 6 and 7 cannot be hit by the hammer directly, the motions of each bridge foot were extracted from measurements on the corpus: F6 is the average result of FA and FB, and the average of FC and FD was used to give F7. The response acceleration was measured at the C string corner of the bridge by the accelerometer. Therefore the measurements relevant to the seven different marker points on the bridge can be obtained, and then used for calculating the planar motion of the cello bridge as will be described next.

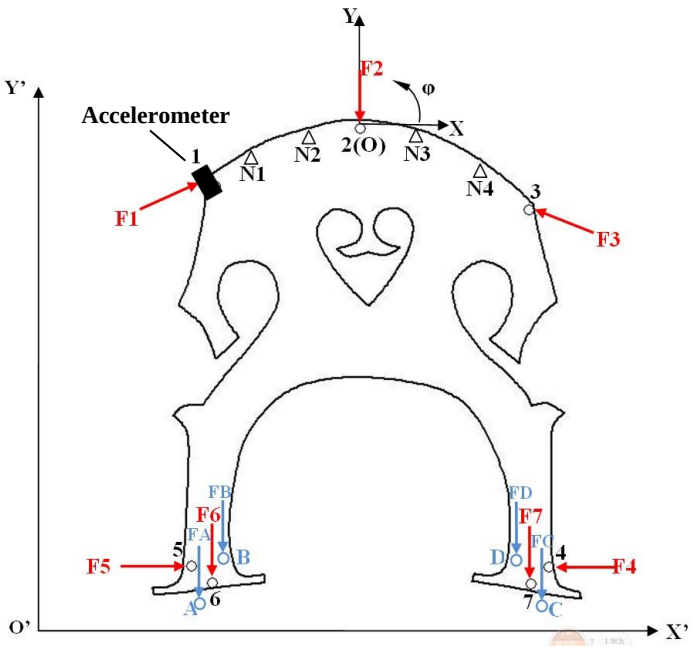

Figure 2 Force response positions and directions for the nine marker points on a cello bridge.

4 CALCULATION OF THE BRIDGE MOTION

Although the motion of the bridge is complex, the bridge can be approximated as a rigid body with little internal deformation over the low- and mid-frequency range, from past research. These planar rigid body motions of the bridge can be described, at any given instant of time, by rotation about a unique point. The location of this point is specific for each frequency and is referred to as the instantaneous centre of rotation. In this subsection, a simple least-squares derivation will be performed to calculate the instantaneous centre of rotation of the cello bridge.

Consider the original position of the cello bridge within a plane coordinate system X'-Y'-φ as indicated in Figure 2. The axis Y' is parallel to the direction of F2 and X' is perpendicular to Y' which is located in the same plane. An anticlockwise rotation φ is considered to be a positive rotation. Take Point 2 labelled as (x_2', y_2') as an example. Denoting the angle between the axis X' and the direction of the applied hammer impact at this point as φ, the coefficients for Point 2 can be written as (x_2', y_2', φ_2). The coefficients of the seven marker points in X'-Y'-φ coordinates can thus be written:

$$M' = \begin{bmatrix} x_1' & y_1' & \varphi_1 \\ x_2' & y_2' & \varphi_2 \\ x_3' & y_3' & \varphi_3 \\ x_4' & y_4' & \varphi_4 \\ x_5' & y_5' & \varphi_5 \\ x_6' & y_6' & \varphi_6 \\ x_7' & y_7' & \varphi_7 \end{bmatrix}.$$

The corresponding coefficients for the four string notches in X'-Y'-φ coordinates are:

$$N' = \begin{bmatrix} x_8' & y_8' & \varphi_8 \\ x_9' & y_9' & \varphi_9 \\ x_{10}' & y_{10}' & \varphi_{10} \\ x_{11}' & y_{11}' & \varphi_{11} \end{bmatrix}.$$

Point 2 is arbitrarily chosen as the reference point for calculating the motion of the bridge. We construct another set of rectangular axes and a rotation angle at Point 2 to resolve any inclined forces and response into the components in Figure 2: the axis Y is in the opposite direction to the hammer force on point 2; the axis X is the direction perpendicular to Y in the same plane; and φ remains the same as that in X'-Y'-φ coordinate system. Thus rewrite the coefficients of the seven marker points and four string notches in X-Y-φ coordinates using formulae:

$$\begin{aligned} x_j &= x_j' - x_2', \\ y_j &= y_j' - y_2', \\ \varphi_j &= \varphi_j, \end{aligned}$$

where j = 1, 2, ..., 11.

Thus in X-Y-φ coordinates,

$$\begin{aligned} x_2 &= 0, \\ y_2 &= 0, \\ \varphi_2 &= \varphi_2. \end{aligned}$$

Now consider the cello bridge as a rigid body which has both translational and rotational motion as illustrated in Figure 3. The plane coordinates X-Y are based on Point 2, now denoted as O, and the marker point P_j labelled as (x_j, y_j) in the X-Y-φ coordinate system rotates about the instantaneous centre C at the instant considered.

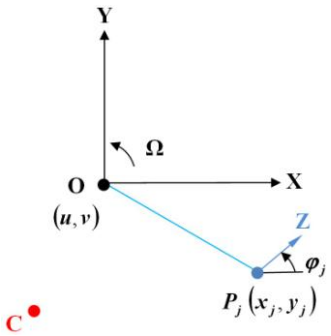

Figure 3 Reference point and one marker point rotate about the instantaneous centre.

It is convenient to introduce the third orthogonal component of the coordinate system. Thus write the velocity vector $\overline{U}$ at O as $(u, v, 0)$, and the angular velocity vector $\overline{\Omega}$ as $(0, 0, \Omega)$. The position vector $\overline{P_j}$ of the marker point P_j is $(x_j, y_j, 0)$, and the angle between the axis X and the direction of measured displacement on the point P_j is φ_j. The velocity vector $\overline{V_j}$ of the point P_j is then defined by the transformation

$$\overline{V_j} = \overline{U} + \overline{\Omega} \times \overline{P_j}$$

where $\overline{V_j}$ is $(u_j, v_j, 0)$ and j = 1, 2, ..., 7. Thus the components of $\overline{V_j}$ at the point P_j can be written

$$u_j = u - \Omega y_j,$$
$$v_j = v + \Omega x_j.$$

Denoting $\overline{Z_j}$ as the unit vector along the direction of the displacement of the marker point P_j,

$$\overline{Z_j} = (\cos\varphi_j, \sin\varphi_j).$$

The translation of point P_j along $\overline{Z_j}$ per unit time is then given by

$$\begin{aligned} t_j &= \overline{V_j} \cdot \overline{Z_j} \\ &= (u - \Omega y_j)\cos\varphi_j + (v + \Omega x_j)\sin\varphi_j \\ &= u\cos\varphi_j + v\sin\varphi_j + \Omega(-y_j\cos\varphi_j + x_j\sin\varphi_j). \end{aligned}$$

Thus the translations of point P_j per unit time in the X-Y-φ coordinate system around the instantaneous centre of rotation can be written as

$$t_j = A_j S,$$

where

$$S = \begin{bmatrix} u & v & \Omega \end{bmatrix}^T,$$

and

$$A_j = \begin{bmatrix} \cos\varphi_j & \sin\varphi_j & -y_j\cos\varphi_j + x_j\sin\varphi_j \end{bmatrix}.$$

The displacements of the seven marker points in the X-Y-φ coordinate system around the instantaneous centre C at that moment can be written by expanding the above A_j to obtain

$$A = \begin{bmatrix} \cos\varphi_1 & \sin\varphi_1 & -y_1\cos\varphi_1 + x_1\sin\varphi_1 \\ \cos\varphi_2 & \sin\varphi_2 & -y_2\cos\varphi_2 + x_2\sin\varphi_2 \\ \cos\varphi_3 & \sin\varphi_3 & -y_3\cos\varphi_3 + x_3\sin\varphi_3 \\ \cos\varphi_4 & \sin\varphi_4 & -y_4\cos\varphi_4 + x_4\sin\varphi_4 \\ \cos\varphi_5 & \sin\varphi_5 & -y_5\cos\varphi_5 + x_5\sin\varphi_5 \\ \cos\varphi_6 & \sin\varphi_6 & -y_6\cos\varphi_6 + x_6\sin\varphi_6 \\ \cos\varphi_7 & \sin\varphi_7 & -y_7\cos\varphi_7 + x_7\sin\varphi_7 \end{bmatrix}.$$

The reciprocal theorem for a linear system has been utilized here: the response collected from Point 1 caused by force applying on a marker point should be the same as that acquired with inverse input and output points. Therefore, the experimental results can be regarded as the vibration responses measured on the seven different marker points along the directions of the original input forces respectively while the input force was exerted on Point 1. Therefore the measured displacements of the seven points along the direction of their input forces in the X'-Y'-φ coordinate system are

$$M = \begin{bmatrix} m_1 & m_2 & m_3 & m_4 & m_5 & m_6 & m_7 \end{bmatrix}^T.$$

Now we can explicitly estimate the velocity vector $\overline{U}$ and rotation rate $\overline{\Omega}$ at O by using the simple least-square solution. The best fit to

$$AS \approx M$$

is given by

$$S = \left(A^T A\right)^{-1} A^T M.$$

The instantaneous centre is now defined by the condition that there is no linear velocity at that point, requiring

$$\overline{U} = \overline{\Omega} \times (-\overline{C})$$

where $\overline{C} = \left(x_{ic}, y_{ic}, 0\right)$: x_{ic} and y_{ic} are the coordinates of the instantaneous centre C in X'-Y'-φ coordinates. Then x_{ic} and y_{ic} can be found straightforwardly:

$$x_{ic} = -v/\Omega,$$
$$y_{ic} = u/\Omega.$$

The coordinates of the instantaneous centre C in the X'-Y'-φ coordinate system are thus

$$x_{ic}' = x_2' - v/\Omega,$$
$$y_{ic}' = y_2' + u/\Omega.$$

The final complication is that the results discussed are all complex numbers. This means that the instantaneous centre moves cyclically during each period of oscillation at the given frequency. If there is a phase difference between the translational and rotational motion components, as there usually is, this trajectory is a straight line that goes to infinity and back from the opposite direction: the distance along the line follows a tangent function. However, there is a well-defined sense of the position on the line where most time is spent (given by the zero of the tangent function), and that is the position that will be plotted when results are shown in the next section.

5 RESULTS

Motions of the tested cello bridge obtained by this least-squares solution are shown in the following two figures. A first look at the instantaneous centre of the tested cello bridge can be seen in Figure 4. The red line shows the X' coordinate of this motion centre at each frequency over the range from 65Hz to 2000 Hz. The upper blue line shows the position of the soundpost foot of the cello bridge while the bottom blue one denotes the bass-bar foot. Figure 5 illustrates the trajectories of the instantaneous centre of the tested cello bridge over a series of frequency ranges ranging in total from 65Hz to 2000 Hz. In each plot, the seven marker points around the bridge are denoted by black circles, the four string notches are denoted by blue circles and the instantaneous centre at each frequency by red circles. It can be seen from these two figures that the instantaneous centre tends to move back and forth between the two feet of the bridge: it falls predominantly on the sound-post side in the frequency range from 65 Hz to 205 Hz, then moves towards the bass-bar side in the frequency range from 205 to 466 Hz, clusters in the middle of two feet over the frequency range from 466 Hz to 1200 Hz, and finally moves back to the sound-post side before 2000 Hz. Only in the highest range shown here does the instantaneous centre move upwards from near the top plate surface.

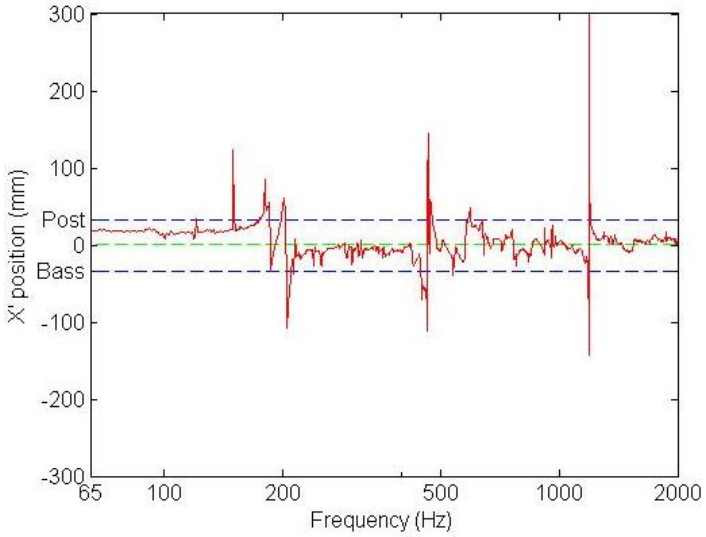

Figure 4 X' coordinates of the instantaneous centre of the tested cello bridge over the frequency range from 65Hz to 2000 Hz.

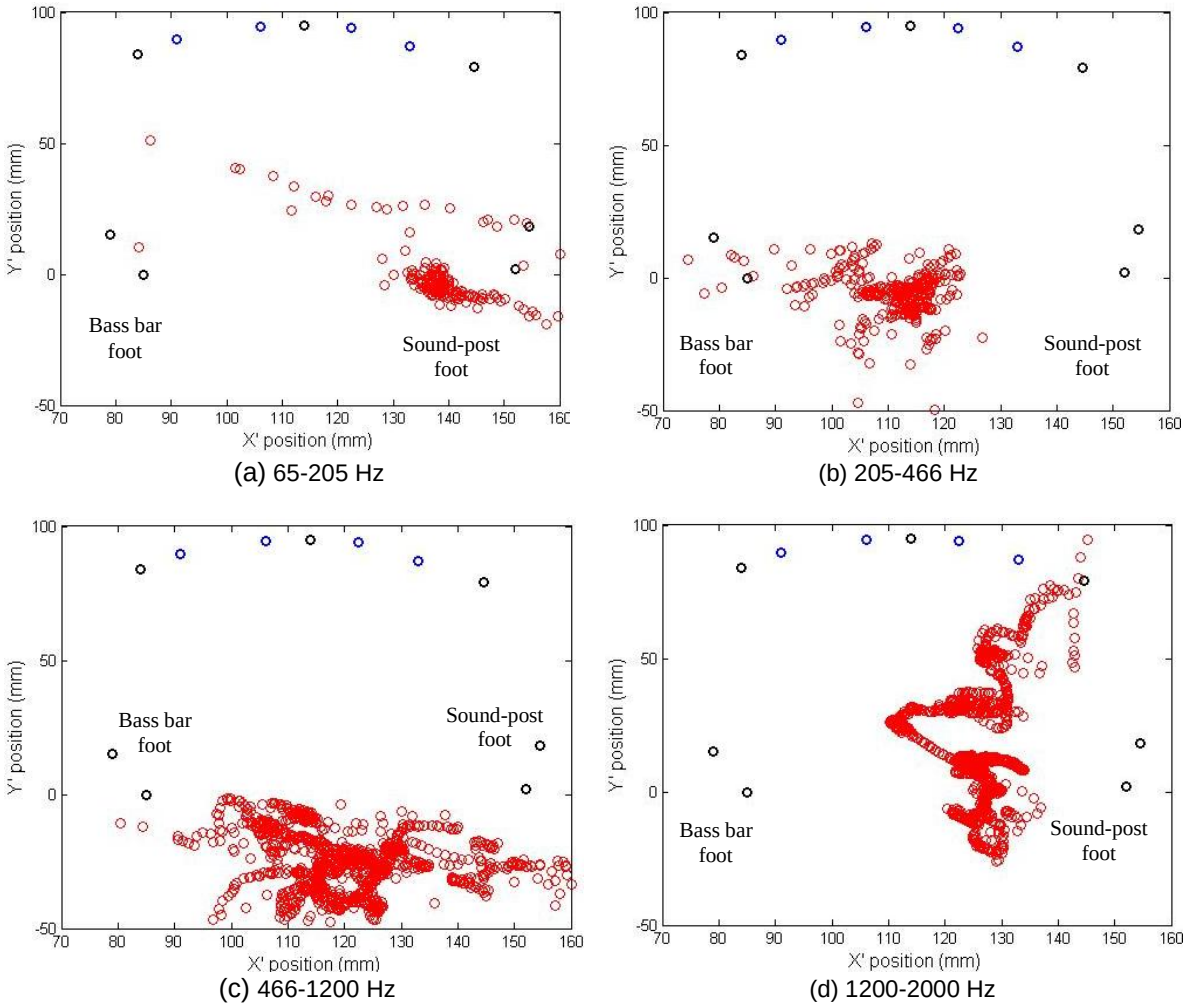

Figure 5 Trajectories of the instantaneous centre of the tested cello over the frequency range from 65Hz to 2000 Hz.

6 CONCLUSIONS

Measurements have been shown that elucidate the detailed motion of a cello bridge at low frequencies. The results are broadly in agreement with behaviour seen in earlier experimental studies. The observed bridge motion shows the characteristics of a rigid body in the low- to mid-frequency range: the bridge pivots around an instantaneous centre with little deformation. The instantaneous centre tends to lie close to the bridge foot near the soundpost at the lowest frequencies, but at higher frequencies it moves towards the bass-bar foot.

The results shown here all relate to one particular cello and bridge, but similar experiments have been carried out on three different cellos with different bridges, with broadly similar conclusions. The experimental results go some way towards explaining the variations between the input admittance of the cello body felt by the separate strings at their respective bridge notches. This in turn bears upon variations in playability from string to string via the response of low body modes to bowing the different strings; for example, variations in minimum bow force and “wolfiness”.

7 REFERENCES

1. C. M. Hutchins and V. Benade, ‘Research papers in violin acoustics 1975-1993’, Vol. I, ASA Woodbury (1997).
2. M. Minnaert and C.C. Vlam, ‘The vibrations of the violin bridge’, Physica, 4(5) 361-372. (1937).
3. B. Bladier, ‘On the bridge of the violoncello’, Compt. Rend. 250 2161-2163. (Mar 1960).
4. W. Reinicke, ‘Übertragungseigenschaften des Streichinstrumentensteges’, J. Catgut. Acoust. Soc. NL19 26-34. (1973).
5. H.A. Müller, ‘The function of the violin bridge’, J. Catgut. Acoust. Soc. NL31 19-22. (1979).
6. L. Cremer: The physics of the violin, MIT Press, Cambridge, MA, 204-208. (1984).
7. W.J. Trott, ‘The violin and its bridge’, J. Acoust. Soc. Am. 81(6) 1948-1954. (1987).
8. K.D. Marshall, ‘Modal Analysis of a Violin’, J. Acoust. Soc. Am. 77(2) 695-709. (1985).
9. O.E. Rodgers and T.R. Masino, ‘The effect of wood removal on bridge frequencies’, J. Catgut. Acoust. Soc. 2d ser 1(6) 6-10. (1990).
10. K. Kishi and T. Osanai, ‘Vibration analysis of the cello bridge using the finite element method’, J. Acoust. Soc. Jpn. 47(4) 274-281. (1991).
11. E.V. Jansson, L. Fryden, and G. Mattsson, ‘On tuning of the violin bridge’, J. Catgut. Acoust. Soc. 2d ser 1(6) 11-15. (1990).
12. E.V. Jansson, ‘Experiments with the violin String and bridge’, J. Applied. Acoustics. 30(2) 133-146. (1990).
13. E.V. Jansson, ‘Violin frequency response–bridge mobility and bridge feet distance’, J. Applied. Acoustics. 65(12) 1197-1205. (2004).
14. G. Bissinger, ‘The violin bridge as filter’, J. Acoust. Soc. Am. 120(1) 482-491. (2006).